

A Hydrodynamical Mechanism for Generating Astrophysical Jets

X. Hernandez¹, Pablo. L. Rendón², Rosa G. Rodríguez-Mota², A. Capella³

¹*Instituto de Astronomía, Universidad Nacional Autónoma de México, Apartado Postal 70–264 C.P. 04510 México D.F. México.*

²*Centro de Ciencias Aplicadas y Desarrollo Tecnológico, Universidad Nacional Autónoma de México, Apartado Postal 70–186, México D.F. 04510, México.*

³*Instituto de Matematicas, Universidad Nacional Autónoma de México, México D.F. 04510, México*

Released 28/02/2011

ABSTRACT

We show that if in a classical accretion disk the thin disk approximation fails interior to a certain radius, a transition from Keplerian to radial infalling trajectories should occur. We show that this transition is actually expected to occur interior to a certain critical radius, provided surface density profiles are steeper than $\Sigma(R) \propto R^{-1/2}$, and further, that it probably corresponds to the observationally inferred phenomena of thick hot walls internally limiting the extent of many stellar accretion disks. Once shears stop, the inner region of radially infalling orbits is naturally expected to be cold. This leads to the divergent focusing and concentration of matter towards the very central regions, most of which will simply be swallowed by the central star. However, if a warm minority component is present, we show through a perturbative hydrodynamical analysis, that this will naturally develop into an extremely well collimated and very fast moving pair of polar jets. A first analytic treatment of the problem described is given, proving the feasibility of purely hydrodynamical mechanisms of astrophysical jet generation. The purely hydrodynamic jet generation mechanism explored here complements existing ideas focusing on the role of magnetic fields, which probably account for the large-scale collimation and stability of jets.

Key words: accretion, accretion discs — hydrodynamics — protoplanetary disks — galaxies: jets — ISM: jets and outflows

1 INTRODUCTION

Astrophysical jets occur over a large range of astrophysical scales, from the stellar Newtonian scales of HH objects (e.g. Reipurth & Bally 2001), to the relativistic cases of microquasars and gamma ray bursts (e.g. Mirabel & Rodríguez 1999, Mészáros 2002), to the Mega-parsec extragalactic scales of AGN jets (e.g. Marscher et al. 2002). Although the processes of propagation and collimation appear to be relatively well understood in terms of the interplay between the hydrodynamics of the problem (Scheuer 1997) and magnetic fields (e.g. Blandford 1990), the precise mechanism of jet generation probably remains as the most uncertain part of the system.

Existing jet generation mechanisms focus on the interaction between the rotating material in the inner regions of the accretion disk and the magnetic field of the central (rotating or otherwise) star, or perhaps an external magnetic field threading the disk. See for example Blandford & Payne (1982), Henriksen & Valls-Gabaud (1994), Meier et al. (2001), Price et al. (2003) for some examples. Although

generically successful, detailed comparisons with observations do not always yield consistent results, e.g. Ferreira et al. (2006). Further, the details of relative orientation of stellar spin, accretion disk and magnetic field configurations, have to be supplied in somewhat highly specific manners.

As an alternative, we explore the possibility of hydrodynamical jet generation mechanism where magnetic fields play no rôle, but only the intrinsic hydrodynamical physics of the interplay between the accretion and the central star wholly determine the characteristics of the jet. The main obstacle to such a scheme is the presence of a centrifugal barrier associated with the angular momentum content of the material in the accretion disk. We show however, that the thin disk approximation for accretion disks, which is equivalent to the assumption of quasi-circular orbits for the disk (e.g. Pringle 1981), is expected to break down internal to a certain critical radius, resulting in a transition to quasi-radial flow for the disk. Once this obstacle has been removed, an analytic first order perturbation treatment serves to demonstrate the feasibility of purely hydrodynamical jets. We show also that many generic features of observed astro-

physical jets across a wide range of scales, can be naturally accounted for in the general model presented. The presence of magnetic fields in jet phenomena is evident empirically, however, it is not impossible that their main contribution to the problem could be restricted to the radiation of the jet material and to its long range collimation, with purely hydrodynamical physics playing a part in the actual jet generation mechanisms.

The problem of jet formation has been studied extensively in the context of classical hydrodynamics, most often regarding fluid-body interactions. The appearance of stable coaxial jets resulting from radially-symmetric velocity fields over thin fluid sheets has been established by, among others, Taylor (1960). The rôle played by both the magnitude and the direction of velocity in the formation of this type of jet is the subject of a theoretical study by Glauert (1956), where it is shown that at the point at which the jet forms, a large velocity gradient is observed, and momentum flux is constant, with horizontal momentum being transformed into vertical momentum. Similar results were obtained by King & Needham (1994), who provide an asymptotic study of a jet formed by a vertical plate accelerating into a semi-infinite expanse of stationary fluid of finite depth with a free surface and a gravitational restoring force. It is found that as the fluid approaches the plate in a horizontal direction, a gradual rise in free-surface elevation occurs. Eventually, a thin region is reached where vertical velocity dominates horizontal velocity as a consequence of the fluid finding it more difficult to overcome the inertia it would meet by continuing its horizontal motion than escaping vertically towards the low-pressure free surface. In essence, this same mechanism can allow for jet formation in the context of the problem we study here.

In section 2 we develop the criterion for transition to radial flow in a standard accretion disk. The perturbative solution to the resulting problem of a radially infalling disk is then developed in section 3. Section 4 presents trajectories for particular cases of the solution obtained in the previous section, in dimensionless units. Finally, we give our conclusions in section 5,

2 THE TRANSITION TO RADIAL FLOW

We start from a standard thin accretion disk where material orbits on quasi-circular Keplerian orbits around a central star of mass M . Assuming axial symmetry and cylindrical coordinates, the total angular momentum of a ring at radius R of width ΔR will be:

$$L = 2\pi R^3 \Delta R \Sigma(R) \Omega(R) \quad (1)$$

where Σ and Ω are the surface density and orbital frequency profiles of the disk, respectively. If the breaking torque on a given ring of the disk, due to its exterior ring is denoted by $\tau(R)$, the total breaking torque on the ring at radius R will be:

$$\tau_B = \tau(R + \Delta R) - \tau(R). \quad (2)$$

The rate of change of the angular momentum of the ring in question can now be calculated as:

$$\dot{L} = \tau_B = \frac{d\tau}{dR} \Delta R. \quad (3)$$

If at any radius a substantial fraction of the angular momentum of the ring is lost through viscous torques over an orbital period, the assumption of quasi-circular orbits will break down, and the disk will make a transition to mostly radial orbits. This condition can be stated as:

$$\frac{L}{2\dot{L}} < \frac{2\pi}{\Omega}. \quad (4)$$

Substitution of equations (1) and (2) into the above yields:

$$R^3 \Omega^2 \Sigma < 2 \left(\frac{d\tau}{dR} \right), \quad (5)$$

as the condition for the onset of radial flow in the disk.

We can now introduce a model for the torques in terms of the rate of shear and the effective viscosity ν (e.g. Von Weizsäcker 1943, Pringle 1981) as:

$$\tau = 2\pi R^3 \nu \Sigma \frac{d\Omega}{dR}. \quad (6)$$

Taking $\Omega^2 = GM/R^3$ to substitute the above equation into condition (5) gives

$$(GM)^{1/2} \Sigma < -6\pi \frac{d}{dR} (R^{1/2} \nu \Sigma). \quad (7)$$

To proceed further we can take for example, $\nu = \text{constant}$ and a model for the disk surface density profile of the form:

$$\Sigma = \Sigma_0 \left(\frac{R}{R_0} \right)^{-n}, \quad (8)$$

of the type often used in models of accretion disks when fitted to observations (e.g. Hughes et al. 2009). Use of the two above forms for ν and $\Sigma(R)$ reduces condition(7) to:

$$6\pi\nu(n - 1/2) > (GM R)^{1/2}. \quad (9)$$

The above condition will always be met in any accretion disk with $n > 1/2$, interior to a transition radius R_T given by:

$$R_T = \frac{[6\pi\nu(n - 1/2)]^{1/2}}{GM}. \quad (10)$$

It is interesting that directly observed accretion disks have spectra which when modelled typically yield $n \sim 1$, in general $0 < n < 1.5$, e.g. Hartmann et al. (1998), Lada (2006), Hughes et al. (2009). This leads one to expect the transition to radial flow to occur in many of the stellar accretion disks, interior to radii given by equation (10).

Finally, we can explore the consequences of introducing an α prescription (Shakura & Sunyaev 1973) into condition (9), $\nu = \alpha c H$, where c and H are respectively the sound speed and height of the disk, with α a dimensionless number, yielding the dimensionless condition:

$$\mathcal{M} \left(\frac{R}{H} \right) < 6\pi\alpha(n - 1/2), \quad (11)$$

where \mathcal{M} is the ratio of the Keplerian orbital velocity in the disk to the sound speed in the disk. Although the above condition is only valid for constant ν , it illustrates the equivalence between the assumption of quasi-circular orbits for the material in the disk, and the assumption that the disk is thin. We see that the breakdown of the assumption of quasi-circular orbits (condition 9), corresponds to the point where disk is fat.

Writing \mathcal{M} in astrophysical units as:

$$\mathcal{M} = 1.8 \left(\frac{200K}{T} \right)^{1/2} \left(\frac{50AU}{R} \right)^{1/2} \left(\frac{M}{0.5M_{\odot}} \right)^{1/2}, \quad (12)$$

we see that for values typical of what is observationally inferred for the stellar mass and position and temperature of accretion disk walls in T Tauri protoplanetary disks, those indicated in the above equation (e.g. D'Alessio et al. 2005, Espaillat et al. 2007, Hughes et al 2009), one should expect the breakdown of the thin disk approximation ($\mathcal{M} \gg 1$, e.g. Pringle 1981), and consequently, the transition to radial flow.

Taking typical inferred values for R/H at the wall of ~ 5 (e.g. D'Alessio et al. 2005, Espaillat et al. 2007, Hughes et al 2009), we can now write the condition for the transition to radial flow, locally at the wall, as:

$$10 = 6\pi\alpha(n - 1/2). \quad (13)$$

We see that for a standard value of $n \sim 1$ the above equation implies a reasonable value of $\alpha \sim 1$ at the thick wall, significantly higher than the values of ~ 0.01 and lower, which apply for the body of the thin accretion disk beyond this radius. A substantial increase of α as R/H decreases is expected in any turbulence driven viscosity model for accretion disks, e.g. Firmani, Hernandez & Gallagher (1996), in the context of galactic disks.

In terms of the debate surrounding the inference of inner holes in observed accretion disks, many solutions have been proposed in terms of disk clearing mechanisms; grain growth (e.g. Strom et al. 1989, Dullemond & Dominik 2005), photoevaporation (e.g. Clarke et al. 2001), magnetorotational instability inside-out clearing (e.g. Chiang & Murray-Clay 2007, Dutrey et al. 2008), binarity (e.g. Ireland & Kraus 2008) and planet-disk interactions (e.g. Rice et al. 2003). None of the above is entirely satisfactory, as noted by Hughes et al. (2009), mostly due to their incompatibility with a steady state solution. An alternative solution under the proposed scenario, is that there is no actual disk material clearing, only a transition to radial flow at the thick wall, and consequently a shear-free flow interior to this point. Once the disk heating mechanism is removed, as one should expect from the analysis presented in this section, the inner disk disappears from sight.

3 HYDRODYNAMICAL JET SOLUTIONS

We shall now model the physical situation resulting from the scenario described above as an axially symmetrical distribution of cold matter in free fall towards a central star of mass M . Taking a spherical coordinate system with θ the angle between the positive vertical direction and the position vector \vec{r} we have:

$$\frac{1}{r^2} \frac{\partial(r^2 \rho V)}{\partial r} + \frac{1}{r \sin(\theta)} \frac{\partial(\sin(\theta) \rho U)}{\partial \theta} = 0, \quad (14)$$

$$V \frac{\partial V}{\partial r} + \frac{U}{r} \frac{\partial V}{\partial \theta} - \frac{U^2}{r} = -\frac{1}{\rho} \frac{\partial P}{\partial r} - \frac{GM}{r^2}, \quad (15)$$

$$V \frac{\partial U}{\partial r} + \frac{U}{r} \frac{\partial U}{\partial \theta} + \frac{VU}{r} = -\frac{1}{r\rho} \frac{\partial P}{\partial \theta}, \quad (16)$$

for the continuity equation, and the radial and angular components of Euler's equation. In the above, V , U , ρ and P

give the radial velocity, angular velocity, matter density and pressure, respectively. We have neglected temporal derivatives, as we are interested at this point, in the characteristics of steady state solutions. We take as a background state a free-falling axially symmetrical distribution of cold gas, described by $V_0 = -(2GM/r)^{1/2}$, $U_0 = 0$ and $\nabla \vec{P}_0 = 0$, a consistent solution to eqs.(15) and (16). Having ignored the inclusion of the radius at which the transition to radial flow takes place in the choice of V_0 limits the validity of the analysis to radial scales along the plane of the disk much smaller than R_T . This is justified by the fact that jets appear as phenomena extremely localised towards $R \rightarrow 0$. We now take a density profile given by:

$$\rho_0(r, \theta) = f(r)g(\theta), \quad (17)$$

where $f(r)$ is a dimensionless function of r and $g(\theta)$ describes the polar angle dependence of the infalling material, for example, one can ask for $g(\theta = \pi/2) = \bar{\rho}_0$, diminishing symmetrically towards the poles. The choice of this last function will determine the details of the problem, and can be thought of as something of the type

$$g(\theta) = \bar{\rho}_0 e^{-\left(\frac{\theta - \pi/2}{\sqrt{2}\theta_0}\right)^2} \quad (18)$$

with $\bar{\rho}_0$ a normalisation constant and θ_0 a form constant describing the flattening of the disk of infalling material. However, we shall mostly leave results indicated in terms of $g(\theta)$. The continuity equation (14) now fixes $f(r)$ through:

$$-\frac{g(\theta)}{r^2} \frac{d}{dr} [(2GM)^{1/2} r^{3/2} f(r)] = 0, \quad (19)$$

and hence $f(r)r^{3/2} = cte.$, which completes the description of the background state through:

$$\rho_0(r, \theta) = \left(\frac{\bar{r}}{r}\right)^{3/2} g(\theta), \quad (20)$$

with \bar{r} a constant which determines the point at which $g(\theta = \pi/2) \Rightarrow \rho_0 = \bar{\rho}_0$.

We shall now analyse the behaviour of a fraction of somewhat hotter material, through a first order perturbation analysis of the above solution. This small fraction could represent the last of the material to fully cool, or result from the irradiation of the central star onto the upper and lower surfaces of the radially infalling disk, as described by e.g. Hollenbach et al. (1994) or Alexander et al. (2006) for the standard case of Keplerian accretion disks, in connection with the problem of disk photoevaporation. In the above it is shown that ionizing radiation from the star generically creates an ionized layer on the surface of the disk.

Regarding the evolution of this component, we shall also be interested in a steady state solution given by:

$$V(r, \theta) = V_0(r) + V_1(r, \theta), \quad (21)$$

$$U(r, \theta) = 0 + U_1(r, \theta), \quad (22)$$

$$\rho(r, \theta) = \rho_0(r, \theta) + \rho_1(r, \theta), \quad (23)$$

where quantities with subscript (1) denote the perturbation on the background solution. Writing eqs.(14), (15) and (16) to first order in the perturbation one obtains after rearranging terms:

$$g(\theta) \frac{\partial(r^{1/2} V_1)}{\partial r} - B \frac{\partial(r^{3/2} \rho_1)}{\partial r} = \frac{-1}{r^{1/2} \sin(\theta)} \frac{\partial(\sin(\theta) g(\theta) U_1)}{\partial \theta}, \quad (24)$$

$$\frac{\partial (V_1/r^{1/2})}{\partial r} = \frac{Ar^{3/2}}{g(\theta)} \frac{\partial \rho_1}{\partial r}, \quad (25)$$

$$\frac{\partial (rU_1)}{\partial r} = \frac{Ar^2}{g(\theta)} \frac{\partial \rho_1}{\partial \theta}, \quad (26)$$

In the above we have assumed an isothermal equation of state for the perturbation $P_1 = c^2 \rho_1$, an assumption often used in the modeling of astrophysical jets, e.g. the T Tauri jets observed and modelled by Hartigan et al. (2004). This idealised case serves to illustrate clearly the consequences of the physical setup being considered, as it allows for an analytic solution. The generalisation to more realistic adiabatic, polytropic or otherwise equations of state can be performed numerically, and can be expected to yield qualitatively similar results, although interesting differences in the details can be expected to emerge, which will be considered latter. In the above three equations we have introduced the constants $A = (c^4/2GM\bar{r}^3)^{1/2}$ and $B = (2GM/\bar{r}^3)^{1/2}$.

To make further progress we can attempt a solution through the method of separation of variables, proposing a solution of the form: $V_1 = V_r V_\theta$, $U_1 = U_r U_\theta$, $\rho_1 = \rho_r \rho_\theta$. This ansatz yields two independent systems of three equations each, one for the radial, and one for the angular dependences of the perturbations. The radial equations become:

$$\frac{d(V_r/r^{1/2})}{dr} = C_r r^{3/2} \frac{d\rho_r}{dr}, \quad (27)$$

$$\frac{d(rU_r)}{dr} = C_\theta r^2 \rho_r, \quad (28)$$

$$\frac{d(r^{1/2}V_r)}{dr} - \left(\frac{BC_r}{A}\right) \frac{d(r^{3/2}\rho_r)}{dr} = C_c \frac{U_r}{r^{1/2}}. \quad (29)$$

While the angular ones result in:

$$V_\theta g(\theta) = \left(\frac{A}{C_r}\right) \rho_\theta, \quad (30)$$

$$\frac{d\rho_\theta}{d\theta} = \left(\frac{C_\theta}{A}\right) g(\theta) U_\theta, \quad (31)$$

$$\frac{d(\sin(\theta)g(\theta)U_\theta)}{d\theta} = -C_c \sin(\theta)g(\theta)V_\theta. \quad (32)$$

In splitting the radial and angular dependences of the perturbed continuity equation, eq.(24), we have used the result of the angular equation of the perturbed radial Euler equation, eq.(30). The constants C_r , C_θ and C_c are the separation constants of the problem. Firstly we turn to the angular system, which allows an exact solution.

We can take eq.(32) and substitute into it the product $g(\theta)U_\theta$ from eq.(31), and the product $g(\theta)V_\theta$ from eq.(30) to obtain an equation involving only ρ_θ :

$$\frac{d^2 \rho_\theta}{d\theta^2} + \cot(\theta) \frac{d\rho_\theta}{d\theta} + \left(\frac{C_c C_\theta}{C_r}\right) \rho_\theta = 0, \quad (33)$$

having solution:

$$\rho_\theta = c_1 P_m(\cos(\theta)) + c_2 Q_m(\cos(\theta)). \quad (34)$$

In the above equation c_1 and c_2 are normalisation constants, and P_m and Q_m are the Legendre polynomials of the first and second kinds, respectively. The index of these functions is given by the relation $2m = (4C_T + 1)^{1/2} - 1$, where $C_T = (C_c C_\theta / C_r)$. As typical of separation of variables problems, we see the solution as an eigenvalue problem, with the

separation constants determining the order of the solution function. The requirement of axial symmetry forces m to be even. Any such desired angular distribution for ρ_θ can now be constructed as an infinite series of the above functions. For simplicity we analyse the case of $m = 2$ ($C_T = 6$), $c_1 = \bar{\rho}_\theta$, $c_2 = 0$:

$$\rho_\theta = \bar{\rho}_\theta (3\cos^2(\theta) - 1) \quad (35)$$

This will result in slightly less material along the plane of the disk, and slightly more along the poles, for the total density $\rho = \rho_0 + \rho_1$, with respect to the background state ρ_0 . At this point eqs.(30) and (31) can be used to obtain:

$$V_\theta = \left(\frac{A\bar{\rho}_\theta}{C_r}\right) \left(\frac{3\cos^2(\theta) - 1}{g(\theta)}\right) \quad (36)$$

$$U_\theta = -\left(\frac{6A\bar{\rho}_\theta}{C_\theta}\right) \left(\frac{\cos(\theta)\sin(\theta)}{g(\theta)}\right) \quad (37)$$

The case of the radial system is more cumbersome, as the linear operator which appears is of third order. A good approximation can be obtained by discarding the term on the right hand side of eq.(29), which can then be readily integrated to give:

$$V_r = \left(\frac{BC_r}{A}\right) r \rho_r. \quad (38)$$

In the above we have taken the integration constant which appears as being equal to zero, from requiring $V_r \rightarrow 0$ for $\rho_r \rightarrow 0$. Substituting the above relation for V_r into eq.(27) leads to:

$$\frac{d\rho_r}{dr} \left[\left(\frac{B}{A}\right) r - r^2\right] + \left(\frac{B}{A}\right) \frac{\rho_r}{2} = 0. \quad (39)$$

The second term in the above equation can be dismissed for $r < 2GM/c^2$, which is in any case the validity regime defined by having previously neglected the right hand side of eq.(29), as it is easy to check from the final complete solution. In this regime we now obtain:

$$\rho_r = \bar{\rho}_r \left(\frac{\bar{r}_\rho}{r}\right)^{1/2}, \quad (40)$$

$$V_r = \left(\frac{BC_r}{A}\right) \bar{\rho}_r \bar{r}_\rho^{1/2} r^{1/2}, \quad (41)$$

Where \bar{r}_ρ is a characteristic radius at which $\rho_r = \bar{\rho}_r$. Now from eq.(28),

$$U_r = \left(\frac{2C_\theta \bar{\rho}_r \bar{r}_\rho^{1/2}}{5}\right) r^{3/2}. \quad (42)$$

In the above equation we have also taken the integration constant as zero, from requiring $U_r \rightarrow 0$ for $r \rightarrow 0$. Choosing without loss of generality the two characteristic radii \bar{r} and \bar{r}_ρ both equal to GM/c^2 , we can now write the full solution as:

$$\rho_1 = \bar{\rho}_J \left(\frac{GM}{c^2 r}\right)^{1/2} (3\cos^2(\theta) - 1), \quad (43)$$

$$V_1 = \left(\frac{\bar{\rho}_J}{\bar{\rho}_0}\right) \left(\frac{2c^4 r}{GM}\right)^{1/2} \left(\frac{3\cos^2(\theta) - 1}{g_\theta}\right), \quad (44)$$

$$U_1 = -\left(\frac{12\bar{\rho}_J}{5\bar{\rho}_0}\right) \left(\frac{r}{GM}\right)^{3/2} \left(\frac{c^4 \cos(\theta)\sin(\theta)}{2^{1/2} g_\theta}\right), \quad (45)$$

where we have introduced $\bar{\rho}_J = \bar{\rho}_\theta \bar{\rho}_r$ and g_θ as the angular part of $g(\theta)$, $g(\theta)/\bar{\rho}_0$. The full solution can be seen to depend only on the two parameters $\bar{\rho}_0$ and $\bar{\rho}_J$, normalisation constants for the densities of the background state and the perturbation, with the velocities of the perturbation solution depending only, and linearly, on the ratio $Q = 2^{1/2} \bar{\rho}_J / \bar{\rho}_0$, which is expected to be small, beyond natural dependences on the physical parameters of the problem, M and c .

We see from eq.(45) that the angular velocity will be zero only for $\theta = \pi/2$, $\theta = 0$ and $\theta = \pi$. Thus, movement along the plane of the disk will remain along the plane, but also, along the poles movement will be exclusively radial. This last point, together with the positive sign of the radial velocity along the poles, provides for a well collimated jet along the poles. From eq.(44) we see that one has only to ask for a background state where matter is concentrated on the plane of the disk with relatively empty poles, e.g. $g(\theta) \rightarrow 0$ for $\theta \rightarrow 0$ and $\theta \rightarrow \pi$, in order to obtain extremely large ejection velocities along the poles. The axial symmetry condition imposed on eq.(34) guarantees both axial symmetry and symmetry above and below the plane of the disk for the full solution. We see also that if one takes higher orders for m , the index of the Legendre polynomial solution to eq.(33), one obtains increasingly more critical angles at positions intermediary between 0 and $\pi/2$ at which the angular velocity goes to zero. In fact, more complex geometries and asymmetric jets appear, as inferred observationally by e.g. Ferreira et al. (2006), if m is taken as an arbitrary real number. However, modelling a situation where a polar jet dominates the ejection identifies $m = 2$ as the leading order.

Notice that the qualitative behaviour of the solution is guaranteed by the exactness of the angular solution, the approximation $r < 2GM/c^2$ used for solving the radial problem will only introduce an error in the actual values of the radial velocities outside of $r < 2GM/c^2$, but will not change the fact that velocities will be of radial infall along the plane of the disk, $\theta = \pi/2$, and of radial outflow along the poles (where the background solution becomes very small), the jet solution for $\theta = 0, \pi$.

The two constants of the problem, $\bar{\rho}_0$ and $\bar{\rho}_J$, can now be calculated once a choice of $g(\theta)$ is specified, from the two conditions:

$$\dot{M}_a = 2\pi \int_0^\pi \rho_0 V_0 \sin(\theta) r^2 d\theta, \quad (46)$$

$$\dot{M}_j = 2\pi \int_0^{\theta_J} \rho_1 V_1 \sin(\theta) r^2 d\theta, \quad (47)$$

where θ_J is a suitable angle defining the opening of the jet, in all likelihood very small, as will be seen in the following section. In the above equations \dot{M}_a gives the matter accretion rate onto the central star, and \dot{M}_j the matter ejection rate due to the jet. Dimensionally, the two quantities above will scale as:

$$\dot{M}_a = C_a \frac{(\pi GM)^2}{c^3} \bar{\rho}_0 \quad (48)$$

$$\dot{M}_j = C_j \frac{(\pi GM)^2}{c^3} \frac{\bar{\rho}_J^2}{\bar{\rho}_0}, \quad (49)$$

where C_a and C_j are two dimensionless constants which will depend on the choice of g_θ , and which would be expected to be of order 1.

Qualitatively, this type of model naturally furnishes a tight disk-jet connection (c.f. eq. 44) e.g., as now firmly established in microquasars and AGN jets (see e.g. Marscher et al. 2002, Chatterjee et al. 2009). In the above systems bursts of enhanced jet activity are seen to follow temporal dips in disk luminosity output after small characteristic delay times. In the present model, such a situation would be expected if the critical radius for transition to radial flow in the disk made a sudden transition to higher values. Again, the drop in disk output might not reflect the disk material disappearing (in this case being swallowed by the central black hole, as sometimes proposed), but simply fading from view as heating mechanisms shut down, then naturally enhancing jet activity as the effective \dot{M}_a increases.

4 PARTICULAR SOLUTIONS

In order to present a sample of the trajectories expected in the model, we turn to the full solution to the problem, eqs.(21) and (22), but written in dimensionless form:

$$\frac{d\mathcal{R}}{d\mathcal{T}} = \frac{-1}{\mathcal{R}^{1/2}} + Q\mathcal{R}^{1/2} \left(\frac{3\cos^2(\theta) - 1}{g_\theta} \right), \quad (50)$$

$$\frac{d\theta}{d\mathcal{T}} = -\frac{6}{5} Q\mathcal{R}^{1/2} \left(\frac{\sin(\theta)\cos(\theta)}{g_\theta} \right). \quad (51)$$

The above remain in spherical coordinates, where $\mathcal{R} = rc^2/GM$ and $\mathcal{T} = tc^3/GM$. A choice of Q and g_θ now allows to numerically integrate trajectories. We take $Q = 5 \times 10^{-2}$, and

$$g_\theta = e^{-\left(\frac{\theta - \pi/2}{\sqrt{2}\theta_0}\right)^2} \quad (52)$$

with $\theta_0 = 0.38$ radians, or about 22 degrees. This value is far from representing an extremely flattened disk, and hence one which does not force the jet solution, see eq.(44). With these parameters, and initial conditions specified in dimensionless cylindrical coordinates as $R = 2$ and Z ranging from 0.4 to 1.4, we solve eqs.(50) and (51) through a finite differences scheme to plot figure 1. For this case, the two lowermost curves present trajectories which all turn downwards to converge onto the central star. These are solutions which essentially follow the background state, infalling onto the bottom of the potential well. As one raises the initial value of Z however, a threshold is crossed and curves of a very different type ensue, the six upper jet trajectories shown in figure 1. We see the large pressure gradients associated with the distribution of matter in the background solution acting to break the fall of the incoming material, turn it back, and then accelerate it vertically through the vertical density gradients. These jet trajectories present a relatively constant thickening at the base of the jet of order $R = 0.5$, which then rapidly diminishes with height to eventually yield an extremely collimated structure which rapidly narrows to below the resolution limit of the solution, notice the horizontal displacement of the vertical axis.

Note also that although the region beyond $\mathcal{R} = 2$ lies outside the approximation of the radial solution, the quali-

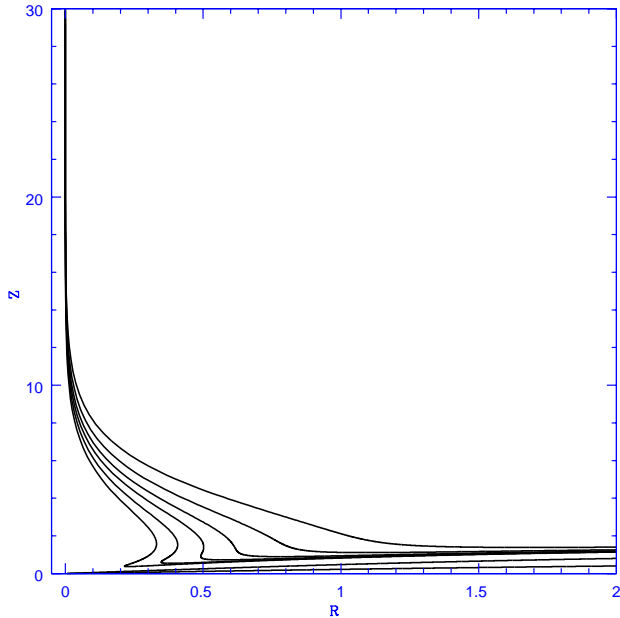


Figure 1. The figure gives trajectories for the complete solution, for a range of initial vertical height positions at $R = 2$. The dimensionless parameter of the problem was chosen as $Q = 5 \times 10^{-2}$. We see the lowermost two trajectories converging into the central potential, but the six upper ones shooting up into a polar jet, where velocities are over 4 orders of magnitude higher than what was originally present along the disk.

tative form of the full solution will not deviate much from what is shown in figure 1, due to the exact character of the angular solution. The final well collimated jet ejecting material along the poles will be a generic feature.

We can also measure the velocities along the jet, which scale linearly with the value of Q , and are sensitive to the choice of g_θ and in this case θ_0 . For the cases presented here values upwards of $10^3 c$ commonly appear along the jet, much larger than the values of order c present in the disk. These radial velocities are somewhat inexact, but will always present large values for background state configurations which empty towards the poles (c.f. eq.44), and will present larger values as the vertical density gradients increase. Notice that the generic validity of the solution proposed does not require that all of the disk material should lose all of its angular momentum at the critical radius R_T , only that some of the disk material should lose most of its angular momentum at that point. Any minor, residual angular momentum remaining on the disk fraction which forms the jet will only establish a finite jet cross-sectional area through the appearance of a centrifugal barrier, which will present only a small correction on the scenario given here. Still, the empirical presence of spectroscopically studied accretion disks truncated interior to certain critical radii suggests the very substantial reduction of the shears in that region, as will be the case when a transition to radial flow takes place.

In going back to eqs.(50) and (51) we see that one expects

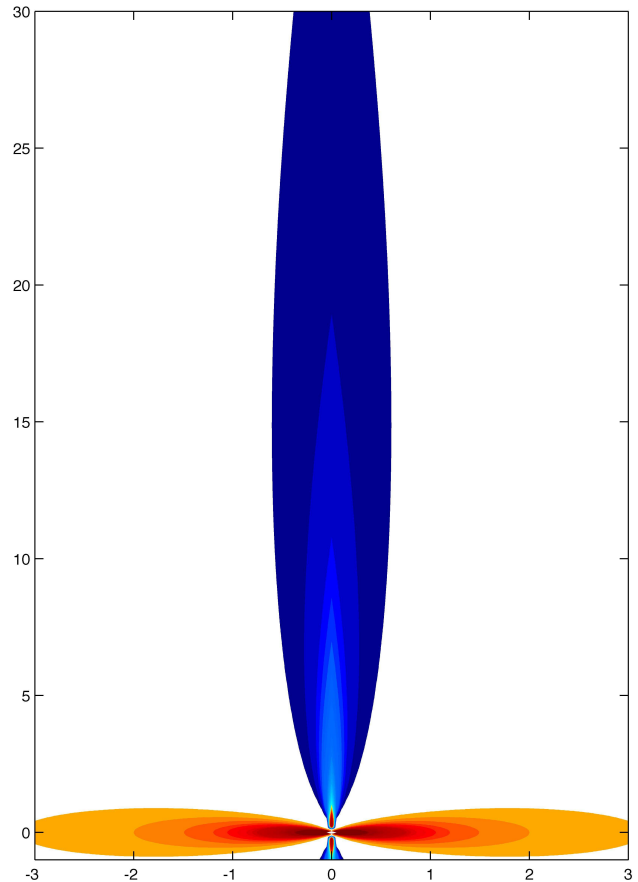


Figure 2. The figure gives trajectories for the complete solution, for a range of initial vertical height positions at $R = 3.0$. The dimensionless parameter of the problem was chosen as $Q = 10^{-4}$. We see a very thin disk developing a central bulge inwards of $R = 1$, from which an extremely well collimated jet of very fast material exits along the poles.

$$Q^2 \sim \frac{\dot{M}_j}{\dot{M}_a}. \quad (53)$$

It is reassuring that for the jets associated with T Tauri stars for example, values of \dot{M}_j/\dot{M}_a of between 0.1 and 0.01 on average are observationally inferred and therefore of order $0.3 < Q < 0.1$ (e.g Hartigan et al. 1996, Gullbring et al. 1998, Hartigan et al. 2004, Ferreira et al. 2006). These are compatible with the value of $Q = 5 \times 10^{-2}$ used to plot fig. (1), and hence ones which will readily yield jet solutions. Given the substantial spread in the inferred values quoted above, we see that values of 10^{-3} or even 10^{-4} occur. We note that for smaller values of Q the jet becomes more centrally localised, making the numerical problem of integrating trajectories challenging. In general, thin disk jet solutions will appear for lower values of Q , or conversely, jet solutions for low values of Q require thinner disks, small values of θ_0 , for the function g_θ used in the example.

Figure 2 presents an example with a much smaller value of $Q = 10^{-4}$, requiring a slightly thinner disk with $\theta_0 = 0.24$, close to 14 degrees. The figure shows a contour plot for dimensionless momentum flow, the product of the dimensionless velocity, $d\mathcal{R}/dT$, and density in units of M/\mathcal{R}^3 from eqs. (43) and (44). Within the disk contours span the from -8 to -0.1 , in intervals of 0.05, while in the jet contours

span from 2×10^{-4} to 10^{-2} in intervals of 5×10^{-5} . The disk appears clearly identified as being made up of infalling material, while the jet shows up as a region of pure outflow carrying little mass, but at velocities of order $10^5 c$. Again, we see the main features of the solution being well established in the region interior to $R < 2$, the details of the radial part of the solution beyond this region will be somewhat off, within the qualitative solution shown.

The long range stability and coherence of these structures lies outside the scope of this work, and is in all probability furnished by a series of mechanisms extensively explored in the literature including angular momentum, magnetic fields and pressure containment of the surrounding medium, e.g. Begelman et al. (1984), Blandford (1990), Falle (1991), Kaiser & Alexander (1997).

In going to the more extreme jet phenomena associated with stellar black holes (e.g. Mirabel & Rodriguez 1999), quasars (e.g. Marscher 2002) and gamma ray bursts (e.g. Mészáros 2002), it is natural to expect the ideas presented here to apply, but amplified to a much more extreme regime by the appearance of corresponding relativistic and general relativistic effects, to first order, the shift in the divergence in the potential from $r = 0$ in the Newtonian case to $r = r_s$ in the general relativistic one. It is therefore natural to expect purely hydrodynamic jet generation mechanism to apply across all classes of astrophysical objects, specially given the qualitative scalings and similarities which appear over all astrophysical jet classes (e.g. Mirabel & Rodriguez 1999, Mendoza, Hernandez & Lee 2005), in addition to the magnetically driven processes traditionally found in the literature.

Notice from eq.(44) the intimate link between the jet velocity and the physical state of the infalling material, c and \dot{M}_a through $\bar{\rho}_0$. This implies that temporal variations in the parameters of the infalling disk will result in temporal variations in the density and velocity of the jet material, in a way described by eqs.(43) and (44). The above can serve as a physical description of the key processes relevant to the formation of internal shocks in astrophysical jets, the main ingredient behind phenomena such as HH objects and gamma ray bursts.

5 CONCLUSIONS

We show that given a radially infalling accretion disk, a purely hydrodynamical jet ensues.

We calculate the condition for the transition from quasi-circular to quasi-radial flow in a standard accretion disk, and show it will always occur for power law surface density profiles of the form $\Sigma \propto R^{-n}$, interior to a critical radius, provided $n > 1/2$.

Comparison with inferred inner holes in observed accretion disks yields results consistent with our estimates for the above transition radius, the point where shears in the flow (and hence heating) end.

Well collimated jets readily appear, proving the existence of purely hydrodynamical mechanisms for the generation of astrophysical jets.

ACKNOWLEDGEMENTS

Xavier Hernandez acknowledges the hospitality of the Observatoire de Paris for the duration of a sabbatical stay during which many of the ideas presented here were first developed. Pablo Rendon and Rosa Rodriguez acknowledge financial support from project PAPIIT IN110411 DGAPA UNAM. Antonio Capella acknowledges financial support from project PAPIIT IN101410 DGAPA UNAM.

REFERENCES

- Alexander, R. D., Clarke, C. J., Pringle, J. E., 2006, MNRAS, 369 229
 Begelman, M. Blandford, R. D., Rees, M., 1984, Rev. Mod. Phys., 56, 256
 Blandford, R. D., Payne, D. G., 1982, MNRAS, 199, 883
 Blandford, R. D., 1990, in "Active Galactic Nuclei, eds. Courvoisier, T. L., Mayor, M., Saas-Fee Advanced Course 20 (Les Diablerets: Springer-Verlag), 161-275
 Chatterjee, R., et al., 2009, ApJ, 704, 1689
 Chiang, E., Murray-Clay, R., 2007, Nat. Phys., 3, 604
 Clarke, C. J., Gendrin, A., Sotomayor, M., 2001, MNRAS, 328, 485
 D'Alessio, P., et al., 2005, ApJ, 621, 461
 Dullemond, C. P., Dominik, C., 2005, A&A, 434, 971
 Dutrey, A., et al., 2008, A&A, 490, L15
 Falle, S. A. E. G., 1991, MNRAS, 250, 581
 Ferreira, J., Dougados, C., Cabrit, S., 2006, A&A, 453, 785
 Firmani, C., Hernandez, X., Gallagher, J., 1996, A&A, 308 403
 Glauert, M. B., 1956, J. Fluid Mech., 1, 625
 Gullbring, E., Hartmann, L., Briceño, C., Calvet, N., 1998, ApJ, 492, 323
 Hartmann, L., Calvet, N., Gullbring, E., D'Alessio, P., 1998, ApJ, 495, 385
 Hartigan, P., Edwards, S., Gandhour, L., 1995, ApJ, 452, 736
 Hartigan, P., Edwards, S., Pierson, R., 2004, ApJ, 609, 261
 Henriksen, R. N., Valls-Gabaud, D., 1994, MNRAS, 266, 681
 Hollenbach, D., Johnstone, D., Lizano, S., Shu, F., 1994, ApJ, 428, 654
 Hughes, A. M., Wilner, D. J., Calvet, N., D'Alessio, P., Claussen, M. J., Hogerheijde, M. R., ApJ, 2007, 664, 536
 Hughes, A. M., et al., 2009, ApJ, 698, 131
 Ireland, M. J., Kraus, A. L., 2008, ApJ, 678, L59
 Keiser, C. R., Alexander, P., 1997, MNRAS, 286, 215
 King, A. C., Needham, D. J., 1994, J. Fluid Mech., 268, 89
 Lada, C., et al., 2006, AJ, 131, 1574
 Marscher, A. P., Jorstad, S. G., Gomez, J., Aller, M. F., Teräsranta, H., Lister, M. L., Stirling, A. M., 2002, Nature, 417, 625
 Meier, D. L., Koide, S., Uchida, Y., 2001, Science, 291, 84
 Mendoza, S., Hernandez, X., Lee, W. H., 2005, Rev. Mex. Astron. Astrofis., 41, 61
 Mészáros, P., 2002, ARA&A, 40, 137
 Mirabel, I. F., Rodriguez, L. F., 1999, ARA&A, 37, 409
 Price, D. J., Pringle, J. E., King, A. R., 2003, MNRAS, 339, 1223
 Pringle, J. E., 1981, ARA&A, 19, 137
 Reipurth, B., Bally, J., 2001, ARA&A, 39, 403
 Rice, W. K. M., Wood, K., Armitage, P. J., Whitney, B. A., Bjorkman, J. E., 2003, MNRAS, 324, 79
 Shakura, N. I., Sunyaev, R. A., 1973, A&A, 24, 337
 Scheuer, P. A. G., 1974, MNRAS, 166, 513
 Strom, K. M., Strom, S. E., Edwards, S., Cabrit, S., Skrutskie, M. F., 1989, AJ, 97, 1451
 Taylor, G., 1960, Proc. R. Soc. Lond. A, 259, 1
 von Weizsäcker, C. F., 1943, Z. Astrophys., 22, 319